Chapter 21
Positive Electrodes in Lithium Systems

21.1 Introduction

Several types of lithium batteries are used in a variety of commercial products, and are produced in very large numbers. According to various reports, the sales volume in 2008 is approximately 10 billion dollars per year, and it is growing rapidly. Most of these products are now used in relatively small electronic devices, but there is also an extremely large potential market if lithium systems can be developed sufficiently to meet the requirements for hybrid, or even plug-in hybrid vehicles.

As might be expected, there is currently a great deal of interest in the possibility of the development of improved lithium batteries in both the scientific and technological communities. An important part of this activity is aimed at the improvement of the positive electrode component of lithium cells, where improvements can have large impacts upon the overall cell performance.

However, before giving attention to some of the details of positive electrodes for use in lithium systems, some comments will be made about the evolution of lithium battery systems in recent years.

Modern advanced battery technology actually began with the discovery of the high ionic conductivity of the solid phase $NaAl_{11}O_{17}$, called sodium beta alumina, by Kummer and coworkers at the Ford Motor Co. laboratory [1]. This led to the realization that ionic transport in solids can actually be very fast, and that it might lead to a variety of new technologies. Shortly thereafter, workers at Ford showed that one can use a highly conducting solid electrolyte to produce an entirely new type of battery, using molten sodium at the negative electrode and a molten solution of sodium in sulfur as the positive electrode, with the sodium-conducting solid electrolyte in between [2].

This attracted a lot of attention, and scientists and engineers from a variety of other fields began to get interested in this area, which is so different from conventional aqueous electrochemistry, in the late 1960s. This concept of a liquid electrode, solid electrolyte (L/S/L) system was quite different from conventional S/L/S

R.A. Huggins, *Energy Storage*, DOI 10.1007/978-3-319-21239-5_21

batteries. The development of the Na/$NiCl_2$ "Zebra" battery system, which has since turned out to be more attractive than the Na/Na_xS version, came along somewhat later [3–5]. This is discussed elsewhere in this text.

As might be expected, consideration was soon given to the possibility of analogous lithium systems, for it was recognized that an otherwise equivalent lithium cell should produce higher voltages than a sodium cell. In addition, lithium has a lower weight than sodium, another potential plus. There was a difficulty, however, for no lithium-conducting solid electrolyte was known that had a sufficiently high ionic conductivity to be used for this purpose.

Instead, a concept employing a lithium-conducting molten salt electrolyte, a eutectic solution of LiCl and KCl that has a melting point of 356 °C, seemed to be an attractive alternative. However, because a molten salt electrolyte is a liquid, the electrode materials had to be solids. That is, the lithium system had to be of the S/L/S type.

Elemental lithium could not be used, because of its low melting point. Instead, solid lithium alloys, primarily the Li/Si and Li/Al systems, were investigated [6], as discussed elsewhere in this text.

A number of materials were investigated as positive electrode reactants at that time, with most attention given to the use of either FeS or FeS_2. Upon reaction with lithium, these materials undergo *reconstitution reactions*, with the disappearance of the initial phases and the formation of new ones [7].

21.2 Insertion Reaction, Instead of Reconstitution Reaction, Electrodes

An important next step was the introduction of the concept that one can reversibly *insert* lithium into solids to produce electrodes with useful potentials and capacities. This was first demonstrated by Whittingham in 1976, who investigated the addition of lithium to the layer-structured TiS_2 to form Li_xTiS_2, where x went from 0 to 1 [8, 9].

Evidence that this insertion-driven solid solution redox process is quite reversible, even over many cycles, is shown in Fig. 21.1, where the charge and discharge behavior of a Li/TiS_2 cell is shown after 76 cycles [10].

Subsequently, the insertion of lithium into a significant number of other materials including V_2O_5, LiV_3O_8, and V_6O_{13} was investigated in many laboratories. In all of these cases, this involved the assumption that one should assemble a battery with pure lithium negative electrodes and positive electrodes with small amounts of, or no, lithium initially. That is, the electrochemical cell is assembled in the charged state.

The fabrication method generally involved the use of glove boxes and a molten salt or organic liquid electrolyte. This precluded operation at high potentials, and the related oxidizing conditions, as discussed elsewhere.

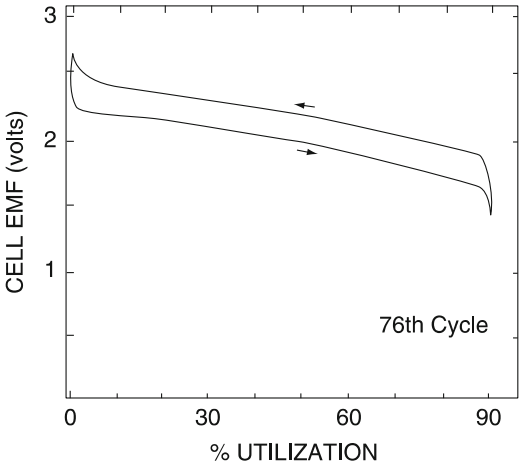

Fig. 21.1 Charge–discharge behavior of a Li/TiS_2 cell after 76 cycles. After ref. [10]

That work involved the study of materials by the addition of lithium, and thus scanned their behavior at potentials lower than about 3 V vs. Li, for this is the starting potential for most electrode materials that are synthesized in air. As lithium is added and the cell is discharged, the potential of the positive electrode goes down toward that of pure lithium.

21.2.1 More Than One Type of Interstitial Site or More Than One Type of Redox Species

The variation of the potential depends upon the distribution of available interstitial places that can be occupied by the Li guest ions. If all sites are not the same in a given crystal structure, the result can be the presence of more than one plateau in the voltage-composition curve. An example of this is the equilibrium titration curve for the insertion of lithium into the V_2O_5 structure shown in Fig. 21.2 [11].

As seen later, similar voltage/composition behavior can result from the presence of more than one species that can undergo a redox reaction as the amount of inserted lithium is varied.

21.3 Cells Assembled in the Discharged State

On the other hand, if a positive electrode material initially contains lithium, and some or all of the lithium is deleted, the potential goes up, rather than down, as it does upon the insertion of lithium. Therefore, it is possible to have positive electrode materials that react with lithium at potentials above about 3 V, if they already contain lithium, and this lithium can be electrochemically extracted.

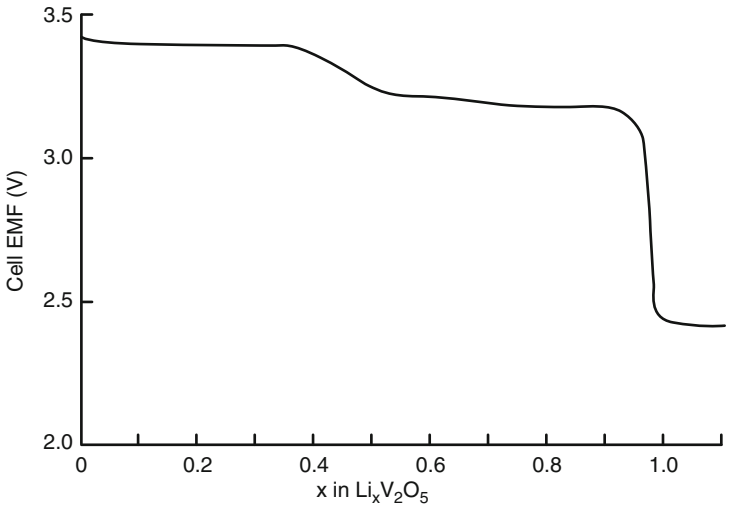

Fig. 21.2 Variation of the potential with the concentration of lithium guest species in the V_2O_5 host structure. After ref. [11]

This concept is shown schematically in Fig. 21.3 for a hypothetical material that is *amphoteric*, and can react at both high and low potentials.

This approach, involving the use of materials in which lithium is already present, was first demonstrated in Prof. Goodenough's laboratory in Oxford. The first examples of materials initially containing with lithium, and electrochemically deleting lithium from them, was the work on $Li_{1-x}CoO_2$ [12] and $Li_{1-x}NiO_2$ [13] in 1980. They showed that it is possible in this way to obtain high reaction potentials, up to over 4 V.

It was not attractive to use such materials in cells with metallic Li negative electrodes, however, and this approach did not attract any substantial interest at that time. This abruptly changed as the result of the surprise development by SONY of a lithium battery containing a carbon negative electrode and a $LiCoO_2$ positive electrode that became commercially available in 1990. These cells were initially assembled in the discharged state. They were activated by charging, whereby lithium left the positive electrode material, raising its potential, and moved to the carbon negative electrode, whose potential was concurrently reduced.

This cell can be represented as

$$Li_xC/\text{organic solvent electrolyte}/Li_{1-x}CoO_2$$

and the cell reaction can be written as

$$C + LiCoO_2 = Li_xC + Li_{1-x}CoO_2 \tag{21.1}$$

This general type of cell and related reaction are most common in commercial cells at the present time.

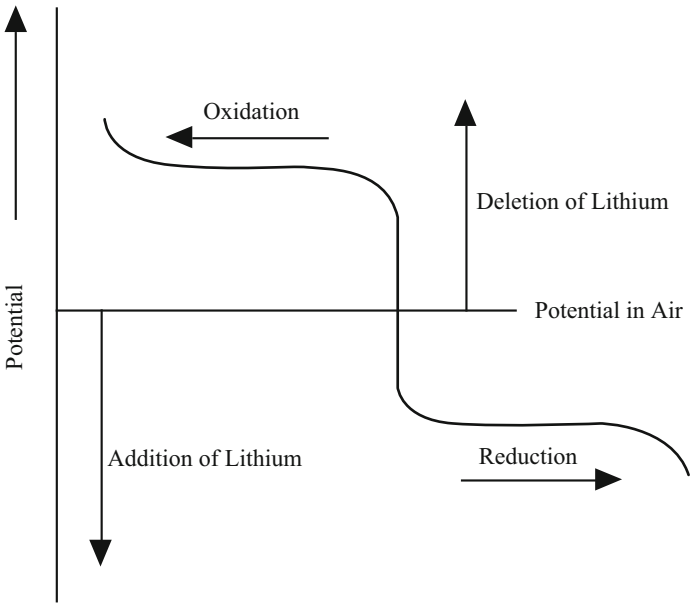

Fig. 21.3 Schematic representation of the behavior of a material that is amphoteric, i.e., that can be both electrochemically oxidized at high potentials by the deletion of lithium, and electrochemically reduced at lower potentials by the addition of lithium

21.4 Solid Positive Electrodes in Lithium Systems

21.4.1 Introduction

In almost every case, the materials that are now used as positive electrode reactants in reversible lithium batteries operate by the use of insertion reactions. This general concept has been discussed several times in this text already. The early ambient temperature lithium battery developments were based upon the observation that lithium could be readily inserted into solids with crystal structures containing available interstitial space. A number of such materials were found, the most notable being TiS_2 and V_6O_{13}. These cells utilized elemental lithium, or lithium alloys, in the negative electrode.

Although precautions had to be taken in preparing and handling the negative materials, due to their propensity to oxidize, the positive electrode materials were typically stable in air.

As the insertion of lithium causes the potential to decrease, and those positive electrodes necessarily operated at potentials lower than that of air, the voltage of such cells was limited to about 3 V.

The shift in concept to the use of air-stable positive electrode materials that already contained lithium, and their operation by the deletion of lithium, led to the

possibility of batteries with significantly higher voltages. But this also required a different strategy for the negative electrodes, for they must be initially devoid of lithium. Cells can be assembled in air in the discharged state. To be put into operation, they must be charged, the lithium initially in the positive electrode being transferred to the negative electrode.

This different approach did not attract any substantial interest until the surprise development by SONY Energytec [14, 15] of a commercial lithium cell that was produced with a $LiCoO_2$ positive electrode, an organic solvent electrolyte, and a carbon negative electrode, i.e., in the discharged state. Upon charging, lithium is transferred from the positive electrode to the carbon negative electrode. Such a cell can be represented simply as

$$Li_xC/\text{organic solvent electrolyte}/Li_{1-x}CoO_2.$$

It is interested that the most commonly used positive electrode in small consumer electronics batteries is now also $LiCoO_2$, although a considerable amount of research is underway in the quest for a more desirable material.

A charge–discharge curve showing the reversible extraction of lithium from $LiCoO_2$ is shown in Fig. 21.4. It is seen that approximately 0.5 Li per mol of $LiCoO_2$ can be reversibly deleted and reinserted. The charge involved in the transfer of lithium ions is balanced by the Co^{3+}/Co^{4+} redox reaction. This process cannot go further, because the layered crystal structure becomes unstable, and there is a transformation into another structure.

Quite a number of materials are now known from which it is possible to delete lithium at high potentials. Some of these are described briefly below, but it is important to realize that this is a very active research area at the present time, and no such discussion can be expected to be complete.

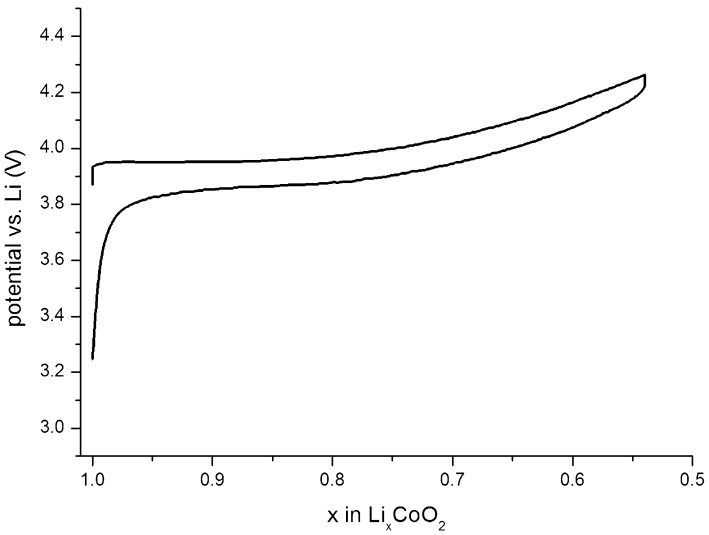

Fig. 21.4 Charge–discharge behavior of Li_xCoO_2

There are a number of interesting materials that have a *face-centered cubic packing* of oxide ions, including both those with the *spinel* structure, e.g., $LiMn_2O_4$, variants containing more than one redox ion, and those with *ordered cation distributions*, which are often described as having *layered structures* (e.g., $LiCoO_2$ and $LiNiO_2$). There also are materials with *hexagonal close packed oxide ion packing*, including some with ordered *olivine-related structures* (e.g., $LiFePO_4$).

In addition, there are a number of interesting materials that have more open crystal structures, sometimes called *framework*, or *skeleton* structures. These are sometimes described as containing *polyanions*. Examples are some sulfates, molybdates, tungstates, and phosphates, as well as Nasicon, and Nasicon-related materials (e.g., $Li_3V_2(PO_4)_3$ and $LiFe_2(SO_4)_3$). In these materials lithium ions can occupy more than one type of interstitial position. Especially interesting are materials with more than one type of polyanion. In some cases the reaction potentials are related to the potentials of the redox reactions of ions in octahedral sites, which are influenced by the charge and crystallographic location of other highly charged ions on tetrahedral sites in their vicinity.

Since the reaction potentials of these positive electrode materials are related to the redox reactions that take place within them, consideration should be given to this matter.

The common values of the formal valence of a number of redox species in solids are given in Table 21.1. In some cases the capacity of a material can be enhanced by the use of more than one redox reaction. In such cases, an issue is whether this can be done without a major change in the crystal structure.

An example of the reaction of lithium with an electrode material containing two redox ions, a Li-Mn-Fe phosphate with the olivine structure, shown in Fig. 21.5 [16].

Not all redox reactions are of practical value in electrode materials, and in some cases, their potentials depend upon their environments within the crystal structure. Some experimental data are presented in Table 21.2.

When lithium or other charged mobile guest ions are inserted into the crystal structure, their electrostatic charge is balanced by a change in the oxidation state of one or more of the redox ions contained in the structure of the host material. The reaction potential of the material is determined by the potential at which this oxidation or reduction of these ions occurs in the host material. In some cases, this redox potential is rather narrowly defined, whereas in others redox occurs over

Table 21.1 Common valences of redox ions in solids

Element	Valences	Valence range	Comments
Ti	2,3,4	2	
V	2,3,4,5	3	
Cr	2,3,6	1	6 is poisonous
Mn	2,3,4,6,7	2	6,7 usable ?
Fe	2,3	1	
Co	2,3	1	
Ni	2,3,4	2	
Cu	1,2	1	

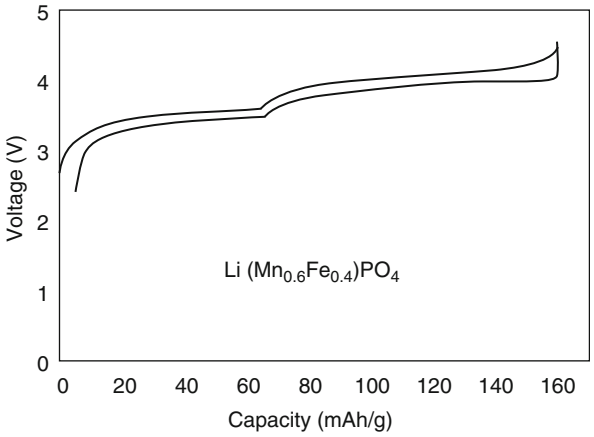

Fig. 21.5 Charge–discharge curve of the reaction of lithium with an example of a double-cation olivine material. After ref. [16]

Table 21.2 Potentials of redox reactions in a number of host materials/volts vs. lithium

Redox System	Nasicon framework phosphates	Layered close-packed oxides	Cubic close-packed spinels	Hexagonal close-packed olivines
V^{2+}/V^{3+}	1.70–1.75			
Nb^{3+}/Nb^{4+}	1.7–1.8			
Nb^{4+}/Nb^{5+}	2.2–2.5			
Ti^{3+}/Ti^{4+}	2.5–2.7		1.6	
Fe/Fe^{2+}	2.65			
Fe^{2+}/Fe^{3+}	2.7–3.0			3.4
V^{3+}/V^{4+}	3.7–3.8			
Mn^{2+}/Mn^{3+}		4.0	1.7	>4.3
Co^{2+}/Co^{3+}		4.2	1.85	>4.3
Ni^{2+}/Ni^{3+}		4.8		>4.3
Mn^{3+}/Mn^{4+}			4.0	
Fe^{3+}/Fe^{4+}	4.4			
Co^{3+}/Co^{4+}			5.0	

a range of potential, due to the variation of the configurational entropy with the guest species concentration, as well as the site distribution.

21.4.2 Influence of the Crystallographic Environment on the Potential

It has been shown that the environment in which a given redox reaction takes place can affect the value of its potential. This matter has been investigated by comparing the potentials of the same redox reactions in a number of oxides with different

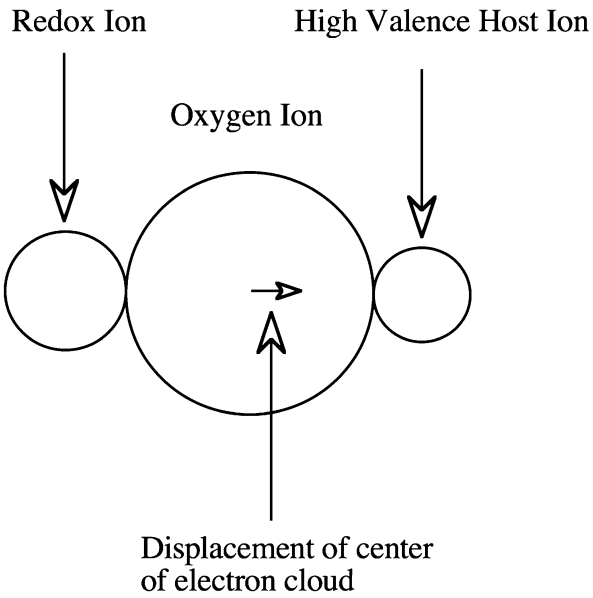

Fig. 21.6 Schematic representation of the displacement of the electron cloud around an oxide ion by the charge upon nearby cations

polyanions, but with the same type of crystal structure. Some of the early references to this topic are listed here [17, 18].

These materials all have crystal structures in which the redox ion is octahedrally surrounded by oxide ions, and the oxide ions also have cations with a different charge in tetrahedral environments on the other side. The electron clouds around the oxide ions are displaced by the presence of adjacent cations with different charges. This is shown schematically in Fig. 21.6.

One of the first cathode materials with a polyanion structure to be investigated was $Fe_2(SO_4)_3$. It can apparently reversibly incorporate up to 2 Li per formula unit, has a very flat discharge curve, indicating a reconstitution reaction, at 3.6 V vs. Li/Li^+ [19, 20].

21.4.3 Oxides with Structures in Which the Oxygen Anions are in a Face-Centered Cubic Array

21.4.3.1 Materials with Layered Structures

As mentioned above, the positive electrode reactant in the SONY cells was Li_xCoO_2, whose properties were first investigated at Oxford [8]. It can be synthesized so that it is stable in air, with $x = 1$. Its crystal structure can be described in terms of a close-packed face-centered cubic arrangement of oxide ions, with the Li^+

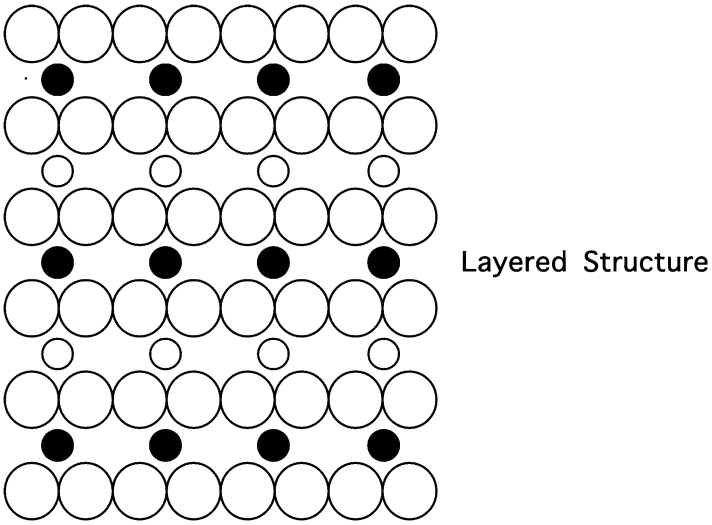

Fig. 21.7 Simplified schematic drawing of a layered structure in which there is alternate occupation of the cation layers between the close-packed oxide ion layers. The solid and open small circles represent two different types of cations. The larger circles are oxide ions

and Co^{3+} cations occupying octahedrally coordinated positions in between layers of oxide ions. The cation positions are ordered such that the lithium ions and the transition metal ions occupy alternate layers between close-packed (111) planes of oxide ions. As a result, these materials are described as having layered, rather than simple cubic, structures. This is shown schematically in Fig. 21.7. However, there is a slight distortion of the cubic oxide stacking because of the difference between the bonding of the monovalent and trivalent cations.

When lithium ions move between octahedral sites within the layers of this structure they must go through nearby tetrahedral sites that lie along the jump path.

$LixCoO_2$ can be cycled many times over the range $1>x>0.5$, but there is a change in the structure and a loss of capacity if more Li+ ions are deleted.

Because it has an inherently lower cost and is somewhat less poisonous, it would be preferable to use $LiNiO_2$ instead of $LiCoO_2$. However, it has been found that Li_xNiO_2 is difficult to prepare with the right stoichiometry, as there is a tendency for nickel ions to reside on the lithium layers. This results in a loss of capacity. It was also found that $LiNiO_2$ readily loses oxygen at high potentials, destroying its layer structure, and tending to lead to safety problems because of exothermic reaction with the organic solvent electrolyte.

There have been a number of investigations of the modification of Li_xNiO_2 by the substitution of other cations for some of the Ni^{3+} ions. It has been found that the replacement of 20–30 % of the Ni^{3+} by Co^{3+} ions will impart sufficient stability [21]. Other aliovalent alternatives have also been explored, including the introduction of Mg^{2+} or Ti^{4+} ions.

In the case of $LiMnO_2$, that also has the alpha $NaFeO_2$ structure, it has been found that if more than 50 % of the lithium ions are removed during charging, conversion to the spinel structure tends to occur. About 25 % of the Mn ions move from octahedral sites in their normal layers into the alkali metal layers, and lithium is displaced into tetrahedral sites [22]. But this conversion to the spinel structure can be avoided by the replacement of half of the Mn ions by chromium [23]. In this case, the capacity (190 mAh/g) is greater than can be accounted for by a single redox reaction, such as Mn^{3+} to Mn^{4+}. This implies that the chromium ions are involved, whose oxidation state can go from Cr^{3+} to Cr^{6+}. Unfortunately, the use of chromium is not considered desirable because of the toxicity of Cr^{6+}.

The replacement of some of the manganese ions in $LiMnO_2$ by several other ions in order to prevent the conversion to the spinel structure has been investigated [24].

A number of other layer-structure materials have also been investigated. Some of them contain two or more transition metal ions at fixed ratios, often including Ni, Mn, Co, and Al. In some cases, there is evidence of ordered structures at specific compositions and well-defined reaction plateaus, at least under equilibrium or near-equilibrium conditions. This indicates reconstitution reactions between adjacent phases.

There have been several investigations of layer phases with manganese and other transition metals present. A number of these, including $LiMn_{1-y}Co_yO_$, have been found to not be interesting, as they convert to the spinel structure rather readily.

However, the manganese–nickel materials, $Li_xMn_{0.5}Ni_{0.5}O_2$ and related compositions, have been found to have very good electrochemical properties, with indications of a solid solution insertion reaction in the potential range 3.5 to 4.5 V vs. Li [25–28]. It appears as though the redox reaction involves a change from Ni^{2+} to Ni^{4+}, whereas the Mn remains as Mn^{4+}. This means that there is no problem with Jahn–Teller distortions, which are related to the presence of Mn^{3+}. The stability of the manganese ions is apparently useful in stabilizing this structure.

At higher manganese concentrations these materials adopt the spinel structure and apparently react by reconstitution reactions, as discussed later in this chapter.

Success with this cation combination apparently led to considerations of compositions containing three cations, such as Mn, Ni, and Co. One of these is $LiMn_{1/3}Ni_{1/3}Co_{1/3}O_2$ [29, 30]. The presence of the cobalt ions evidently stabilizes the layer structure against conversion to the spinel structure. These materials have good electrochemical behavior, and have been studied in many laboratories, but one concern is that they evidently have limited electronic conductivity.

In these materials, as well, when they are fully lithiated, the nickel is evidently predominantly divalent, the cobalt trivalent, and the manganese tetravalent. Thus the major electrochemically active species is nickel, with the cobalt playing an active role only at high potentials. The manganese evidently does not play an active role. It does reduce the overall cost, however.

An extensive discussion of the various approaches to the optimization of the layer structure materials can be found in [31].

21.4.3.2 Materials with the Spinel Structure

The spinel class of materials, with the nominal formula AB_2O_4, has a related structure that also has a close-packed face-centered cubic arrangement of oxide ions. Although this structure is generally pictured in cubic coordinates, it also has parallel layers of oxide ions on (111) planes, and there are both octahedrally-coordinated sites and tetrahedrally-coordinated sites between the oxide ion planes. The number of octahedral sites is equal to the number of oxide ions, but there are twice as many tetrahedral sites. The octahedral sites reside in a plane intermediate between every two oxide ion planes. The tetrahedral sites are in parallel planes slightly above and below the octahedral site planes between the oxide ion planes.

In *normal spinels*, the A (typically monovalent or divalent) cations occupy 1/8 of the available tetrahedral sites, and the B (typically trivalent or quadrivalent) cations 1/2 of the B sites. In *inverse spinels*, the distribution is reversed.

The spinel structure is quite common in nature, indicating a large degree of stability. As mentioned above, there is a tendency for the materials with the layer structures to convert to the closely related spinel structure. This structure is shown schematically in Fig. 21.8.

A wide range of materials with different A and B ions can have this structure, and some of them are quite interesting for use in lithium systems. An especially important example is $Li_xMn_2O_4$. There can be both lithium insertion and deletion from the nominal composition in which $x = 1$. This material has about 10 % less capacity than Li_xCoO_2, but it has somewhat better kinetics and does not have as great a tendency to evolve oxygen.

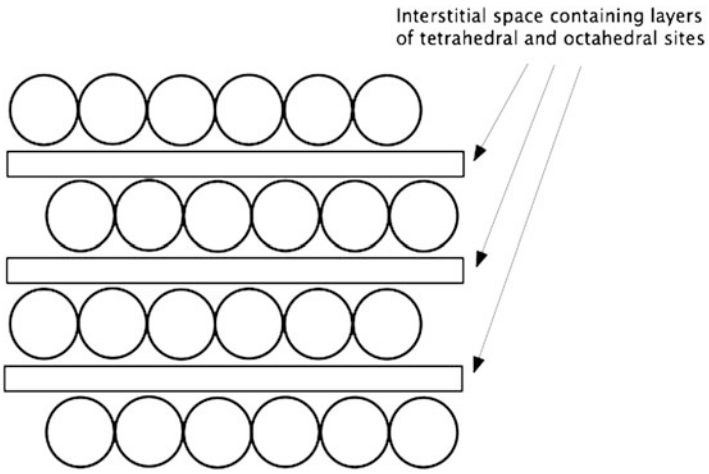

Fig. 21.8 Schematic drawing of the spinel structure in which the cations between the close-packed (111) planes of oxide ions are distributed among both tetrahedral and octahedral sites

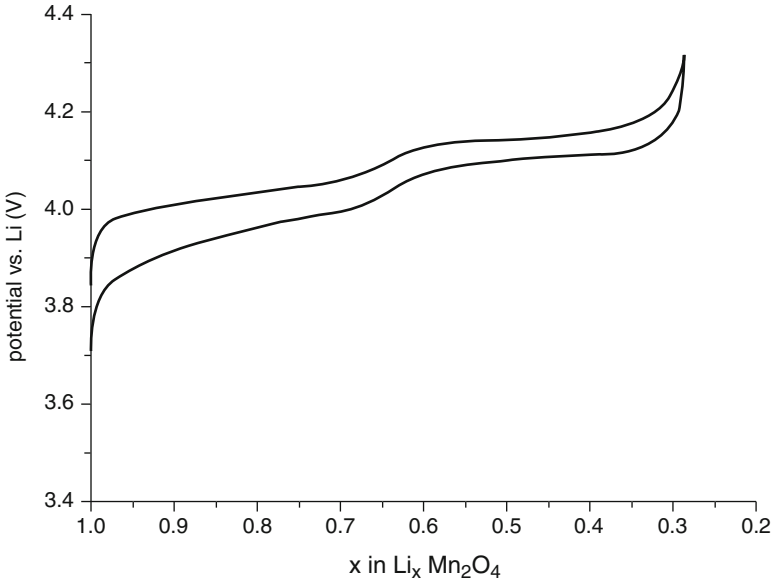

Fig. 21.9 Charge–discharge behavior of $Li_xMn_2O_4$ [32]

$Li_xMn_2O_4$ can be readily synthesized with x equal to unity, and this composition can be used as a positive electrode reactant in lithium batteries. A typical charge–discharge curve is shown in Fig. 21.9.

It is seen that there are two plateaus. This is related to an ordering reaction of the lithium ions on the tetrahedral sites when x is about 0.5.

Although the $Li_xMn_2O_4$ system, first investigated by Thackeray et al. [32, 33], has the inherent advantages of low cost, good kinetics, and being nonpoisonous, it has been found to have some problems that can result in a gradual loss of capacity [34]. Thorough discussions of early work to optimize this material can be found in refs. [35, 36].

One of the problems with this material is the loss of Mn^{2+} into the organic solvent electrolyte as the result of a disproportionation reaction when the potential is low near the end of discharge.

$$2Mn^{3+} = Mn^{4+} + Mn^{2+}. \tag{21.2}$$

These ions travel to the carbon negative electrode, with the result that a layer of manganese metal is deposited that act to block lithium ion transport.

Another problem that can occur at low potentials is the local onset of Jahn–Teller distortion that can cause mechanical damage to the crystal structure. On the other hand, if the electrode potential becomes too high as the result of the extraction of too much lithium, oxygen can escape and react with the organic solvent electrolyte.

These problems are reduced by modification of the composition of the electrode by the presence of additional lithium and a reduction of the manganese [37]. This increase in stability comes at the expense of the capacity. Although the theoretical capacity of $LiMn_2O_4$ is 148 mAh/g, this modification results in a capacity of only 128 mAh/g.

There have also been a number of investigations in which various other cations have been substituted for part of the manganese ions. But in order to avoid the loss of a substantial amount of the normal capacity, it was generally thought at that time that the extent of this substitution must be limited to relatively small concentrations.

At that time the tendency was to perform experiments only up to a voltage about 4.2 V above the Li/Li^+ potential, as had been done for safety reasons when using Li_xCoO_2. But it was soon shown that it is possible to reach potentials up to 5.4 V vs. Li/Li^+ using some organic solvent electrolytes [38, 39].

Experiments on the substitution of some of the Mn^{2+} ions in Li_xMnO_2 by Cr^{3+} ions [40] showed that the capacity upon the 3.8 V plateau was decreased in proportion to the concentration of the replaced Mn ions. But when the potential was raised to higher values, it was found that this missing capacity at about 4 V reappeared at potentials about 4.9 V that was obviously related to the oxidation of the Cr ions that had replaced the manganese ions in the structure. This particular option, replacing inexpensive and nontoxic manganese with more expensive and toxic chromium is, of course, not favorable.

In both the cases of chromium substitution and nickel substitution the sum of the capacities of the higher potential plateau and the lower plateau are constant. This implies that there is a one-to-one substitution, and thus that the oxidation that occurs in connection with the chromium and nickel ions is a one-electron process. This is in contradiction to the normal expectation that these ions undergo a 3-electron (Cr^{3+} to Cr^{6+}) or a two electron (Ni^{2+} to Ni^{4+}) oxidation step.

Another example is work on lithium manganese spinels in which some of the manganese ions have been replaced by copper ions. One of these is $LiCu_xMn_{2-x}O_4$ [41–43]. Investigations of materials in which up to a quarter of the manganese ions are replaced by Cu ions have shown that a second plateau appears at 4.8 to 5.0 V vs. Li/Li^+ that is due to a $Cu^{2+/}Cu^{3+}$ reaction, in addition to the normal behavior of the Li-Mn spinel in the range 3.9 to 4.3 V vs. Li/Li^+ that is related to the Mn^{3+}/Mn^{4+} reaction . Data for this case are shown in Fig. 21.10 [41]. Unfortunately, the overall capacity seems to be reduced when there is a substantial amount of copper present in this material [42]. When x is 0.5 the total capacity is about 70 mAh/g, with only about 25 mAh/g obtainable in the higher potential region.

The redox potentials that are observed when a number of elements are substituted into lithium manganese spinel structure materials are shown in Fig. 21.11 [44].

An especially interesting example is the spinel structure material with a composition $Li_xNi_{0.5}Mn_{1.5}O_4$. Its electrochemical behavior is different from the others, showing evidence of two reconstitution reactions, rather than solid solution behavior [45].

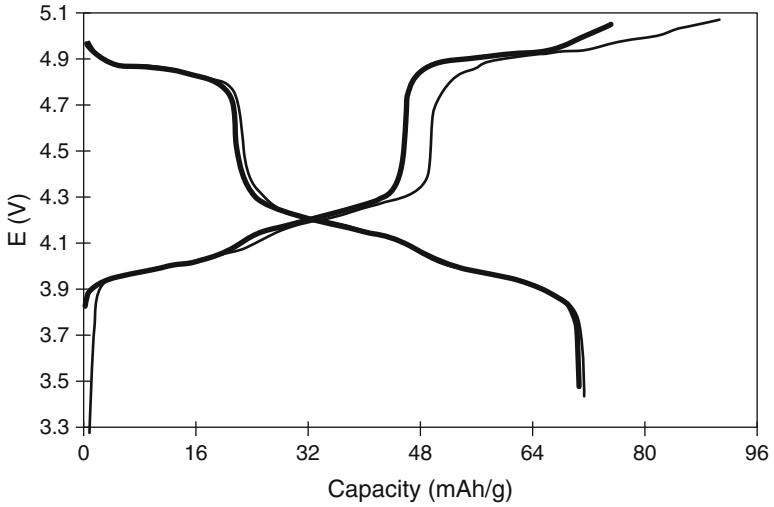

Fig. 21.10 Potential-composition curves for $LiCu_{0.5}Mn_{1.5}O4$. After ref. [40]

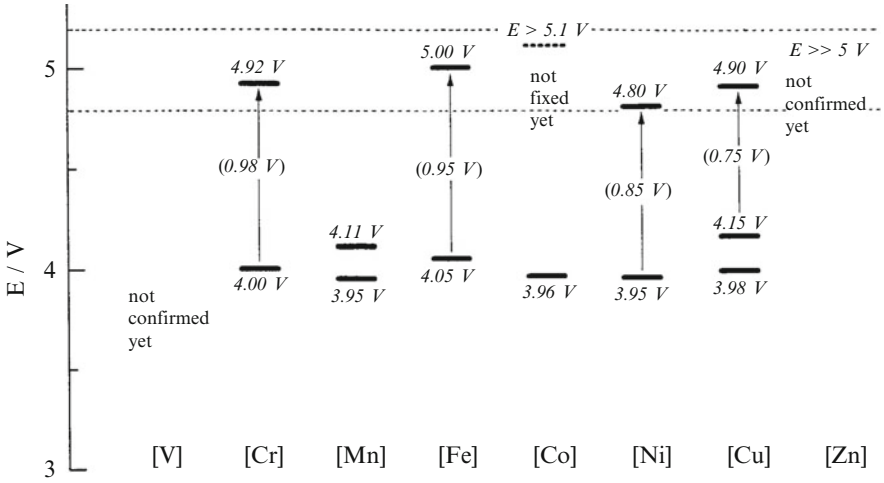

Fig. 21.11 Potential ranges, vs. Li, of redox potentials found as the result of the introduction of a number of cations into lithium manganese spinels. The operating potential range of lithium manganese spinel itself is also shown. After ref. [43]

The constant potential charge–discharge curve for this material in the high potential range is shown in Fig. 21.12 [45]. Careful coulometric titration experiments showed that this apparent plateau is actually composed of two reactions with a potential separation of only 20 mV.

In addition to this high potential reaction, this material also has a reconstitution reaction with a capacity of 1 Li per mol at 2.8 V vs. Li, as well as further lithium

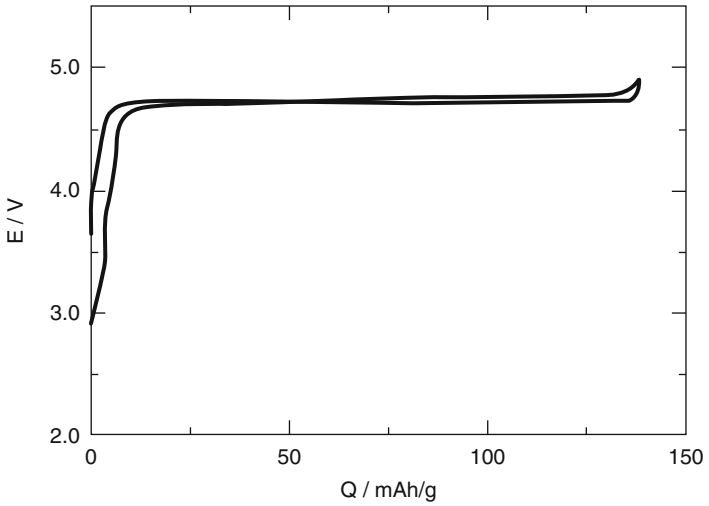

Fig. 21.12 Charge–discharge curves for $Li_xNi_{0.5}Mn_{1.5}O_4$. After ref. [44]

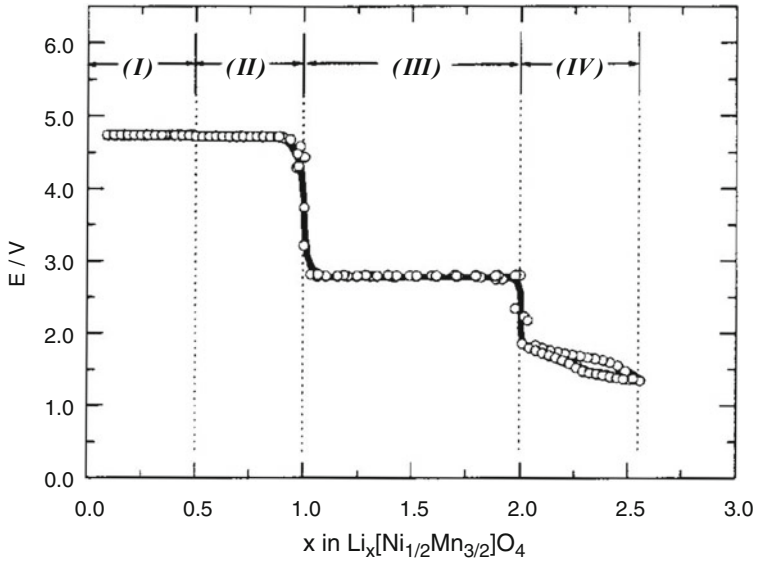

Fig. 21.13 Coulometric titration curve for the reaction of lithium with $Li_xNi_{0.5}Mn_{1.5}O_4$. After ref. [44]

uptake via a single phase reaction below 1.9 V. These features are shown in Fig. 21.13 [45]. It is not fully known what redox reactions are involved in this behavior, but it is believed that those at the higher potentials relate to nickel, and the lower ones to manganese.

21.4.3.3 Lower Potential Spinel Materials with Reconstitution Reactions

Whereas this discussion here has centered on lithium-containing materials that exhibit high potential reactions, and thus are useful as reactants in the positive electrode, attention should also be given to another related spinel structure material that has a reconstitution reaction at 1.55 V vs. Li [46, 47]. This is $Li_{1.33}Ti_{1.67}O_4$, that can also be written as $Li_x[Li_{0.33}Ti_{1.67}O_4]$ for some of the lithium ions share the octahedral sites in an ordered arrangement with the titanium ions. It also sometimes appears in the literature as $Li_4Ti_5O_{12}$.

This spinel structure material is unusual in that there is essentially no change in the lattice dimensions with variation of the amount of lithium in the crystal structure, and it has been described as undergoing a *zero-strain insertion reaction* [48]. This is an advantage in that there is almost no volume change-related hysteresis, leading to very good reversibility upon cycling.

As was mentioned earlier, this material can also be used on the negative electrode side of a battery. Although there is a substantial voltage loss compared to the use of carbons, the good kinetic behavior can make this option attractive for high power applications, where the lithium-carbons can be dangerous because their reaction potential is rather close to that of elemental lithium.

A charge–discharge curve for this interesting material is shown in Fig. 21.14.

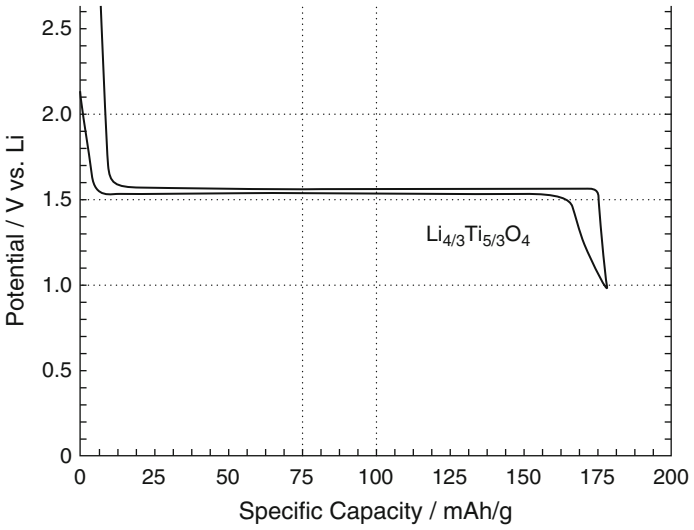

Fig. 21.14 Charge–discharge curve for $Li_4Ti_5O_{12}$. After ref. [46]

21.4.4 Materials in Which the Oxide Ions are in a Close-Packed Hexagonal Array

Whereas in the spinel and the related layered materials such as Li_xCoO_2, Li_xNiO_2, and Li_xMnO_2 the oxide ions are in a cubic close-packed array, there are also many materials in which the oxide ions are in a hexagonal close-packed configuration. Some of these are currently of great interest for use as positive electrode reactants in lithium batteries, but are generally described as having *framework structures*. They are sometimes also called "scaffold," "skeleton," "network," or "polyanion" structures.

21.4.4.1 The Nasicon Structure

The *Nasicon structure* first attracted attention within the solid state ionics community because some materials with this structure were found to be very good solid electrolytes for sodium ions. One such composition was $Na_3Zr_2Si_2PO_{12}$.

This structure has monoclinic symmetry, and can be considered as consisting of MO_6 octahedra sharing corner oxide ions with adjacent XO_4 tetrahedra. Each octahedron is surrounded by six tetrahedral, and each tetrahedron by four octahedra. These are assembled in as a three-dimensional network of M_2X_3 groups. Between these units is three-dimensional interconnected interstitial space, through which small cations can readily move. This structure is shown schematically in Fig. 21.15.

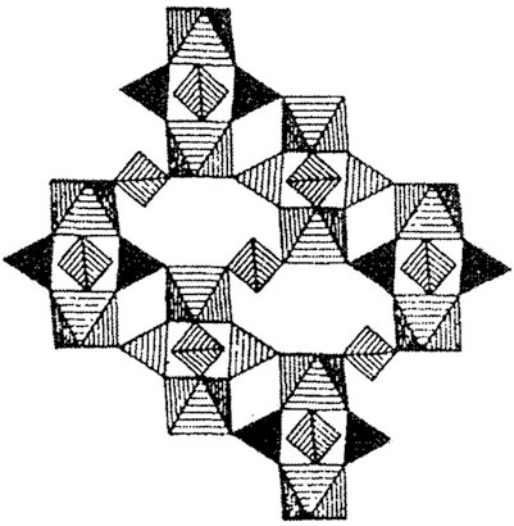

Fig. 21.15 Schematic representation of the Nasicon structure

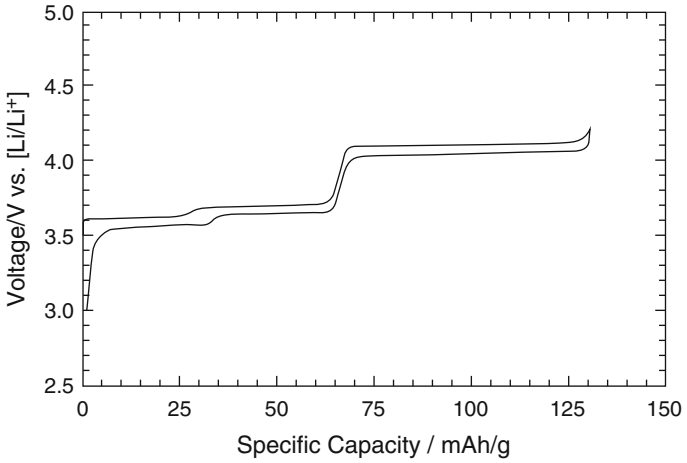

Fig. 21.16 Charge–discharge curve for $Li_3V_2(PO_4)_3$, that has the Nasicon structure. After ref. [50]

Unfortunately, Nasicon was found to not be thermodynamically stable versus elemental sodium, so that it did not find use as an electrolyte in the Na/Na_xS and $Na/NiCl_2$ Zebra cells, that are discussed elsewhere in this text, at that time.

However, by using M cations whose ionic charge can be varied, it is possible to make materials with this same structure that undergo redox reactions upon the insertion or deletion of lithium within the interstitial space. The result is that although Nasicon materials may not be useful for the function for which they were first investigated, they may be found to be useful for a different type of application.

As mentioned earlier, it has been found that the identity of the X ions in the tetrahedral parts of the structure influences the redox potential of the M ions in the adjacent octahedra [17, 49]. This has been called an *induction effect*.

A number of compositions with this structure have been investigated for their potential use as positive electrode reactants in lithium cells [17, 49–51]. An example is $Li_3V_2(PO_4)_3$, whose potential vs. composition data are shown in Fig. 21.16 [51]. The related differential capacity plot is shown in Fig. 21.17.

It is seen that the titration curve shows three two-phase plateaus, corresponding to the extraction of two of the lithium ions in the initial structure. The first two plateaus indicate that there are two slightly different configurations for one of the two lithium ions. The potential must be increased substantially, to over 4 V, for the deletion of the second. Experiments showed that it is possible to extract the third lithium from this material by going up to about 5 V, but that this process is not readily reversible, whereas the insertion/extraction of the first two lithium ions is highly reversible.

These phosphate materials all show significantly more thermal stability than is found in some of the other, e.g., layer- and spinel-structure, positive electrode reactants. This is becoming ever more important as concerns about the safety aspects of high-energy batteries mounts.

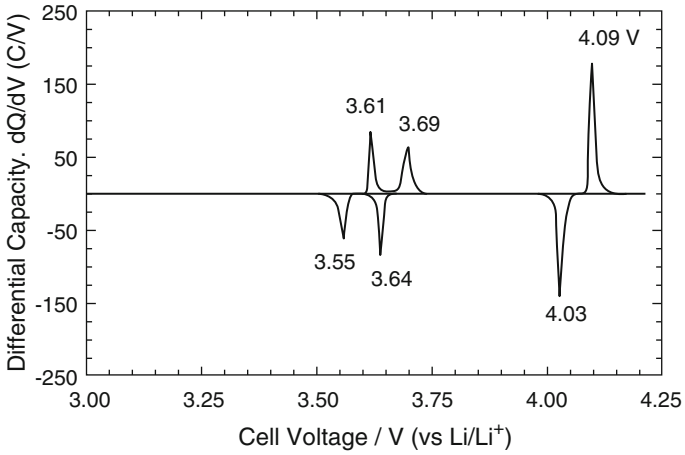

Fig. 21.17 Differential capacity plot corresponding to the charge–discharge data for $Li_3V_2(PO_4)_3$ shown in Fig. 21.10. After ref. [50]

21.4.4.2 Materials with the Olivine Structure

Another group of materials that have a hexagonal stacking of oxide ions are those with the Olivine structure. These materials have caused a great deal of excitement, as well as controversy, in the research community since it was first shown that they can reversibly react with lithium at ambient temperature [52]. The most interesting of these materials is $LiFePO_4$, that has the obvious advantage of being composed of safe and inexpensive materials.

The olivine structure can be described as M_2XO_4, in which the M ions are in half of the available sites of the close-packed hexagonal oxygen array. The more highly charged X ions occupy one eighth of the tetrahedral sites. Thus it is a hexagonal analog of the cubic spinel structure discussed earlier. However, unlike spinel, the two octahedral sites in olivine are crystallographically distinct, and have different sizes. This results in a preferential ordering if there are two M ions of different sizes and/or charges. Thus $LiFePO_4$ and related materials containing lithium and transition metal cations have an ordered cation distribution. The M_1 sites containing lithium are in linear chains of edge-shared octahedral that are parallel to the *c*-axis in the hexagonal structure in alternate a–c planes. The other (M_2) sites are in a zig-zag arrangement of corner-shared octahedral parallel to the *c*-axis in the other a–c planes. The result is that lithium transport is highly directional in this structure.

Experiments showed that extraction of lithium did not readily occur with olivines containing the Mn, Co, or Ni, but proceeded readily in the case of $LiFePO_4$. Deletion of lithium from $LiFePO_4$ occurs by a reconstitution reaction with a moving two-phase interface in which $FePO_4$ is formed at a potential of 3.43 V vs. Li. Although the initial experiments only showed the electrochemical removal of about 0.6 Li ions per mol, subsequent work has shown that greater values can be attained.

A reaction with one lithium ion per mol would give a theoretical specific capacity of 170 mAh/g, which is higher than that obtained with $LiCoO_2$. It has been found that the extraction/insertion of lithium in this material can be quite reversible over many cycles.

These phases have the mineralogical names triphylite and heterosite, although the latter was given to a mineral that also contains manganese. Although this reaction potential is significantly lower than those of many of the materials discussed earlier in this chapter, other properties of this class of materials makes them attractive for application in lithium-ion cells. There is active commercialization activity, as well as a measure of conflict over various related patent matters.

These materials do not tend to lose oxygen and react with the organic solvent electrolyte nearly so much as the layer structure materials, and are they are evidently much safer at elevated temperatures. As a result, they are being considered for larger format applications, such as in vehicles or load leveling, where there are safety questions with some of the other positive electrode reactant materials.

It appeared that the low electronic conductivity of these materials might limit their application, so work was undertaken in a number of laboratories aimed at the development of two-phase microstructures in which electronic conduction within the electrode structure could be enhanced by the presence of an electronic conduction, such as carbon [53]. Various versions of this process quickly became competitive and proprietary.

A different approach is to dope the material with highly charged (supervalent) metal ions, such as niobium, that could replace some of the lithium ions on the small M_1 sites in the structure, increasing the n-type electronic conductivity [54]. On the other hand, experimental evidence seems to indicate that the electronic conduction in the doped Li_xFePO_4 is p-type, not n-type [54, 55]. This could be possible if the cation doping is accompanied by a deficiency of lithium.

This interpretation has been challenged, however, based upon observations of the presence of a highly conductive iron phosphide phase, Fe_2P under certain conditions [56]. Subsequent studies of phase equilibria in the Li-Fe-P-O quaternary system [57] seem to contradict that interpretation.

Regardless of the interpretation, it has been found that the apparent electronic conductivity in these Li_xFePO_4 materials can be increased by a factor of 10^8, reaching values above 10^{-2} S cm^{-1} in this manner. These are higher than those found in some of the other positive electrode reactants, such as $LiCoO_2$ (10^{-3} S cm^{-1}) and $LiMn_2O_4$ (2 to 5×10^{-5} S cm^{-1}).

An interesting observation is that very fine scale cation-doped Li_xFePO4 has a restricted range of composition at which the two phases "LiFePO4" and "FePO4" are in equilibrium, compared to undoped and larger particle-size material [58]. Thus there is more solid solubility in each of the two end phases. This may play an important role in their increased kinetics, for in order for the moving interface reconstitution phase transformation involved in the operation of the electrode to proceed there must be diffusion of lithium through the outer phase to

the interface. The rate of diffusional transport is proportional to the concentration gradient. A wider compositional range allows a greater concentration gradient, and thus faster kinetics.

These materials have been found to be able to react with lithium at very high power levels, greater than those that are typical of common hydride/H_xNiO_2 cells, and commercial applications of this material are being vigorously pursued.

21.4.5 Materials Containing Fluoride Ions

Another interesting variant has also been explored somewhat. This involves the replacement of some of the oxide ions in lithium transition metal oxides by fluoride ions. An example of this is the lithium vanadium fluorophosphate $LiVPO_4F$, that was found to have a triclinic structure analagous to the mineral tavorite, $LiFePO_4{\cdot}OH$ [59]. As in the case of the Nasicon materials mentioned earlier, the relevant redox reaction in this material involves the V^{3+}/V^{4+} couple. The charge–discharge behavior of this material is shown in Fig. 21.18 [60], and the related differential capacity results are presented in Fig. 21.19.

21.4.6 Hybrid Ion Cells

An additional variant involves the use of positive electrode reactants that contain other mobile cations. An example of this were the reports of the use of $Na_3V_2(PO_4)F_3$ as the positive electrode reactant and either graphite [61] or $Li_{4/3}Ti_{5/3}O_4$ [62] as the

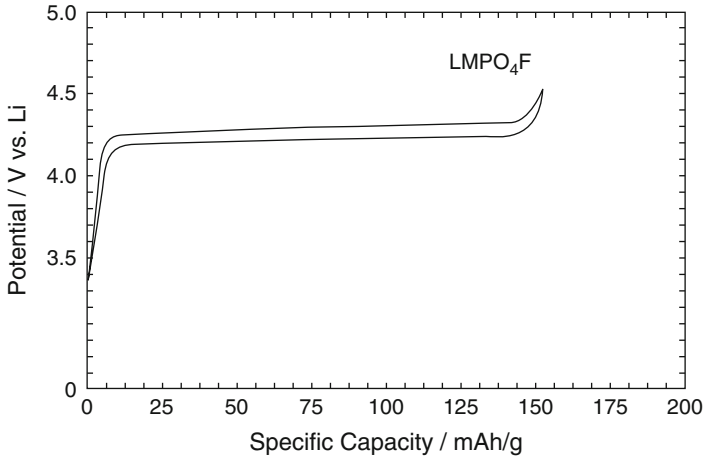

Fig. 21.18 Charge–discharge behavior of $LiVPO_4F$. After ref. [60]

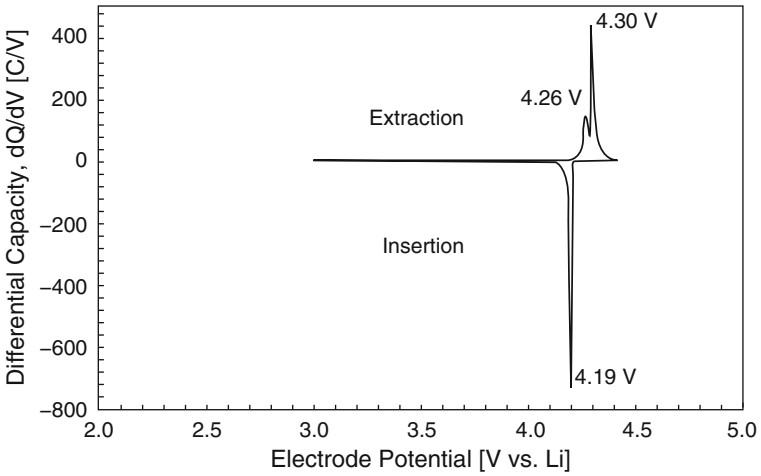

Fig. 21.19 Differential capacity plot corresponding to the charge–discharge data for $LiVPO_4F$ shown in Fig. 20.18. After ref. [60]

negative reactant in lithium-conducting electrolyte cells. It appears as though the mobile insertion species in the positive electrodes gradually shifts from Na^+ to Li^+. Consideration of this type of mixed-ion materials may lead to a number of interesting new materials.

21.4.7 Amorphization

It is pointed out in Chap. 13 that crystal structures can become amorphous as the result of multiple insertion/extraction reactions. A simple explanation for this phenomenon can be based upon the dimensional changes that accompany the variation in the composition. These dimensional changes are typically not uniform throughout the material, so quite significant local shear stresses can result that disturb the regularity of the atomic arrangements in the crystal structure, resulting in regions with amorphous structures. The degree of amorphization should increase with cycling, as is found experimentally.

There is also another possible cause of this effect that has to do with the particle size. As particles become very small, a significant fraction of their atoms actually reside on the surface. Thus the surface energy present becomes a more significant fraction of the total Gibbs free energy. Amorphous structures tend to have lower values of surface energy than their crystalline counterparts. As a result, it is easy to understand that there will be an increasing tendency for amorphization as particles become smaller.

21.4.8 The Oxygen Evolution Problem

It is generally considered that a high cell voltage is desirable, and the more the better, since the energy stored is proportional to the voltage, and the power is proportional to the square of the voltage. However, there are other matters to consider, as well. One of these is the evolution of oxygen from a number of the higher potential positive electrode materials.

There is a direct relationship between the electrical potential and the chemical potential of oxygen in materials containing lithium. In this connection it is useful to remember that the chemical potential has been called the *escaping tendency* in the well-known book on thermodynamics by Pitzer and Brewer.

Experiments have shown that a number of the high potential positive electrode reactant materials lose oxygen into the electrolyte. It is also generally thought that the presence of oxygen in the organic solvent electrolytes is related to thermal runaway and the safety problems that are sometimes encountered in lithium cells. As example of experimental measurements that clearly show oxygen evolution is shown in Fig. 21.20.

The relationship between the potential and the chemical potential of oxygen in electrode materials was investigated a number of years ago, but under conditions that are somewhat different from those in current ambient temperature lithium cells. Nevertheless, the principles are the same, and thus it is useful to review what was found about the thermodynamics of such systems at that time [64].

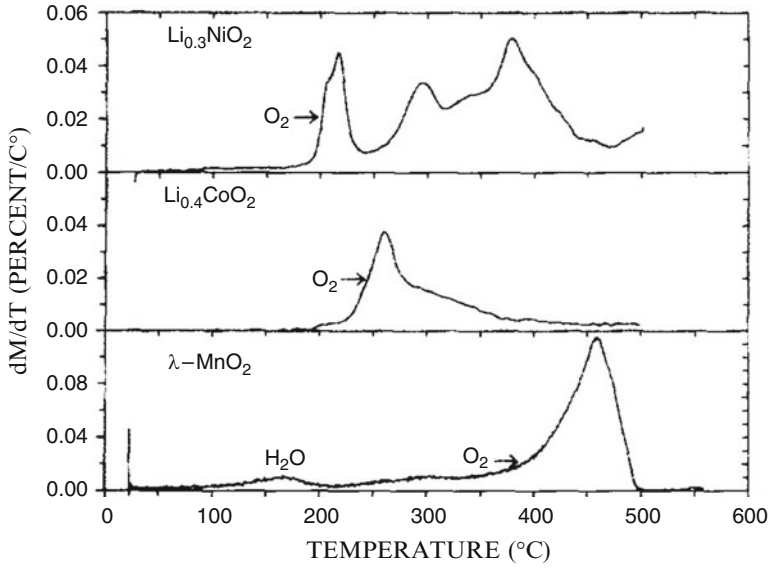

Fig. 21.20 The influence of temperature upon the derivative of the sample weight versus temperature for three different layer structure materials. After ref. [62]

As discussed in this chapter, many of the positive electrode materials in lithium batteries are ternary lithium transition metal oxides. Since there are three kinds of atoms, i.e., three components, present, compositions in these systems can be represented on an Isothermal Gibbs Triangle. As discussed in Chaps. 10 and 12, the Gibbs Phase Rule can be written as

$$F = C - P + 2 \tag{21.3}$$

where F is the number of degrees of freedom, C the number of components, and P the number of phases present. At constant temperature and overall pressure $F = 0$ when $C = P = 3$. This means that all of the intensive variables have fixed values when three phases are present in such three-component systems. Since the electrical potential is an intensive property, this means that the potential has the same value, independent of how much of each of the three phases is present.

It has already been pointed out that the *isothermal phase stability diagram*, an approximation of the Gibbs Triangle in which the phases are treated as though they have fixed, and very narrow, compositions, is a very useful thinking tool to use when considering ternary materials.

The compositions of all of the relevant phases are located on the triangular coordinates, and the possible two-phase tie lines identified. Tie lines cannot cross, and the stable ones can readily be determined from the energy balance of the appropriate reactions. The stable tie lines divide the total triangle into sub-triangles that have two phases at the ends of the tie lines along their boundaries. There are different amounts of the three corner phases at different locations inside the sub-triangles. All of these compositions have the same values of the intensive properties, including the electrical potential.

The potentials within the sub-triangles can be calculated from thermodynamic data on the electrically neutral phases at their corners. From this information it is possible to calculate the voltages versus any of the components. This means that one can also calculate the equilibrium oxygen activities and pressures for the phases in equilibrium with each other in each of the sub-triangles. As was shown earlier, one can also do the reverse, and measure the equilibrium potential at selected compositions in order to determine the thermodynamic data, including the oxygen pressure. The relation between the potential and the oxygen pressure is of special interest because of its practical implications for high voltage battery systems.

The experimental data that are available for ternary lithium–transition metal oxide systems are, however, limited to only three system and one temperature. The Li-Mn-O, Li-Fe-O, and Li-Co-O systems were studied quantitatively using molten salt electrolytes at 400 °C [64]. Because of the sensitivity of lithium to both oxygen and water, they were conducted in a helium-filled glove box. The maximum oxygen pressure that could be tolerated was limited by the formation of Li_2O in the molten salt electrolyte, which was determined to occur at an oxygen partial pressure of 10^{-25} atmospheres at 400 °C. This is equivalent to 1.82 V versus lithium at that temperature. Thus it was not possible to study materials with potentials above 1.82 V versus lithium at that temperature.

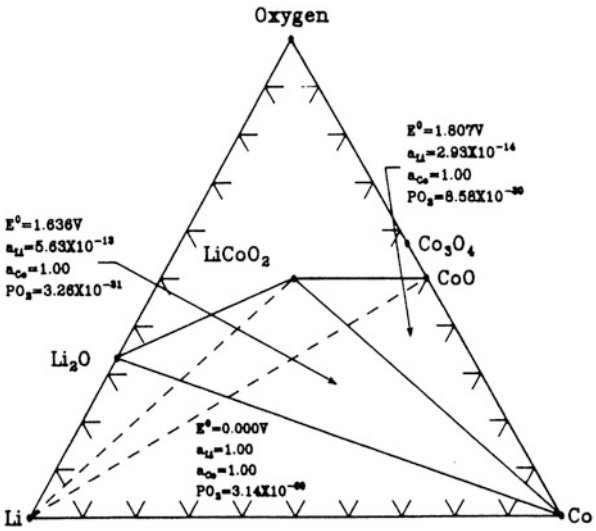

Fig. 21.21 Equilibrium data for the Li-Co-O ternary system at 400 °C. After ref. [63]

As an example, the results obtained for the Li-Co-O system under those conditions are shown in Fig. 21.21 [64], which is also included in Chap. 13.

The general equilibrium equation for a ternary sub-triangle that has two binary transition metal oxides (MO_y and MO_{y-x}) and lithium oxide (Li_2O) at its corners can be written as

$$2x\mathrm{Li} + \mathrm{MO}_y = x\mathrm{Li_2O} + \mathrm{MO}_{y-x} \tag{21.4}$$

According to Hess's law, this can be divided into two binary reactions, and the Gibbs free energy change ΔG_r is the sum of the two

$$\Delta G_r = \Delta G_r^1 + \Delta G_r^2 \tag{21.5}$$

One is the reaction

$$\mathrm{MO}_y = (x/2)\mathrm{O_2} + \mathrm{MO}_{y-x} \tag{21.6}$$

The related Gibbs free energy change is given by

$$\Delta G_r^1 = -\mathrm{RTln}K \tag{21.7}$$

where K is the equilibrium constant.

The other is the formation of Li_2O, that can be written as

$$2x\mathrm{Li} + (x/2)\mathrm{O_2} = x\mathrm{Li_2O} \tag{21.8}$$

for which the Gibbs free energy change is the standard Gibbs free energy of formation of Li_2O.

$$\Delta G_r^2 = x\Delta G_f^o(\mathrm{Li_2}O) \tag{21.9}$$

The potential is related to ΔG_r by

$$E = -\Delta G_r / zF \tag{21.10}$$

that can also be written as

$$E = \mathrm{RT}/(4F)ln(p\mathrm{O_2}) - \Delta G_f^0(\mathrm{Li_2O})/(2F) \tag{21.11}$$

This can be simplified to become a linear relation between the potential E and ln $p(\mathrm{O_2})$, with a slope of RT/(4F) and an intercept related to the Gibbs free energy of formation of Li_2O at the temperature of interest.

Experimental data were obtained on the polyphase equilibria within the subtriangles in the Li-Mn-O, Li-Fe-O, and Li-Co-O systems by electrochemical titration of lithium into various Li_xMO_y materials to determine the equilibrium potentials and compositional ranges. The results are plotted in Fig. 21.22 [64].

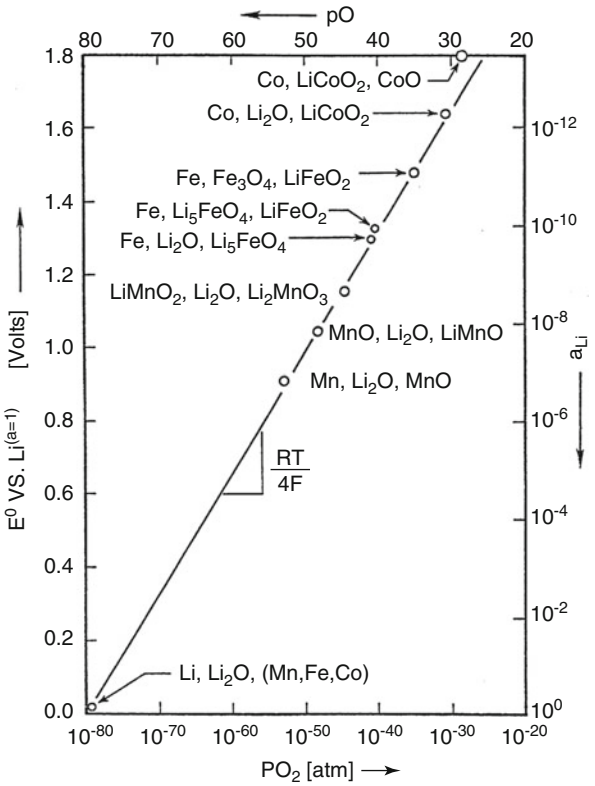

Fig. 21.22 Experimental data on the relation between the potential and the oxygen pressure in phase combinations in the Li-Mn-O, Li-Fe-O, and Li-Co-O systems at 400 °C. After ref. [63]

It is seen that there is a clear correlation between the potentials and the oxygen pressure in all cases. The equation for the line through the data is

$$E = 3.34 \times 10^{-2} \log p(O_2) + 2.65\,V \tag{21.12}$$

The data all fit this line very well, even though the materials involved had a variety of compositions and crystal structures. Thus the relation between the potential and the oxygen pressure is obviously independent of the identity and structures of the materials involved.

Extrapolation of the data in Fig. 21.22 shows that the oxygen pressure would be 1 atmosphere at a potential of 2.65 V vs. Li/Li^+ at 400 °C.

At 25 °C the Gibbs free energy of formation is −562.1 kJ/mol, so the potential at 1 atmosphere oxygen is 2.91 V vs. Li/Li^+. This is about what is observed as the initial open circuit potential in measurements on many transition metal oxide materials when they are fabricated in air.

Evaluating Eq. (21.11) for a temperature of 298 K, it becomes

$$E = 1.476 \times 10^{-2} \log p(O_2) + 2.91\,V \tag{21.13}$$

At this temperature the slope of the potential versus oxygen pressure curve is somewhat less than at the higher temperature. But considering it the other way around, the pressure increases more rapidly as the potential is raised.

This result shows that the equilibrium oxygen pressures in the Li-M-O oxide phases increase greatly as the potential is raised. Values of the equilibrium oxygen pressure as a function of the potential are shown in Table 21.3. These data are plotted in Fig. 21.23.

It can be seen that these values become very large at high electrode potentials, and from the experimental data taken under less extreme conditions, it is obvious

Table 21.3 Values of the equilibrium oxygen pressure over oxide phases in Li-M-O systems at 298 K

E vs. Li/Li^+/V	Logarithm of equilibrium oxygen pressure/atm
1	−129
1.5	−95
2	−62
2.5	−28
3	6
3.5	40
4	73.7
4.5	107.6
5	141.4

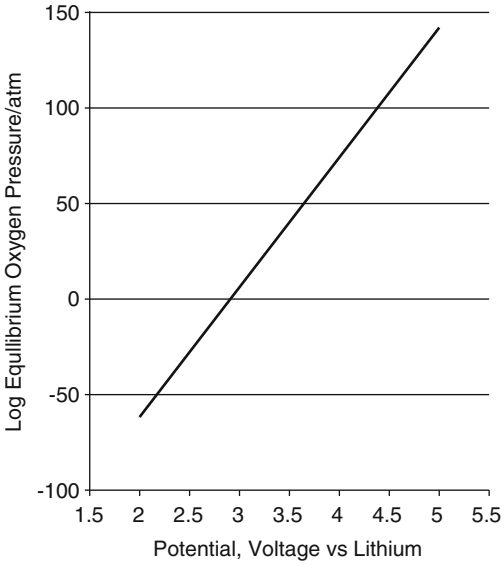

Fig. 21.23 Dependence of the logarithm of the equilibrium oxygen pressure upon the potential in lithium–transition metal oxide systems [63]

that the critical issue is the potential, not the identity of the electrode reactant material or the crystal structure.

One can understand the tendency toward the evolution of oxygen from oxides at high potentials from a different standpoint. Considerations of the influence of the potential on the point defect structure of oxide solid electrolytes has shown that electronic holes tend to be formed at higher potentials, and excess electrons at lower potentials. The presence of holes means that some of the oxide ions have a charge of $1-$, rather than $2-$. That is, they become peroxide ions, O^{-}. This is an intermediate state on the way to neutral oxygens, as in the neutral oxygen gas molecule O_2.

Such ions have been found experimentally on the oxygen electrode surface where the transition between neutral oxygen molecules and oxide ions takes place at the positive electrodes of fuel cells.

21.4.9 Final Comments on This Topic

It is evident that this is a very active research area, with a number of different avenues being explored in the pursuit of higher potentials, greater capacity, longer cycle life, greater safety, and lower cost. It will be interesting to see which of these new materials, if any, actually come into commercial application.

21.5 Hydrogen and Water in Positive Electrode Materials

21.5.1 Introduction

The electrochemical insertion and deletion of hydrogen is a major feature in some important types of aqueous batteries. The use of metal hydrides as negative electrode reactants in aqueous systems is discussed in Chap. 16, and the hydrogen-driven $H_2NiO_2/HNiO_2$ phase transformation is the major reaction in the positive electrode of a number of "nickel" cells, as described in Chap. 17.

It is generally known that alkali metals react vigorously with water, with the evolution of hydrogen. In addition, a number of materials containing lithium are sensitive to air and/or water, and thus have to be handled in dry rooms or glove boxes. Yet most of the lithium-containing oxides now used as positive electrode reactants in lithium battery systems are synthesized in air, often with little heed given to this problem.

It has long been known that hydrogen (protons) can be present in oxides, including some that contain lithium, and that water (a combination of protons and extra oxide ions) can be absorbed into some selected cases. There are several different mechanisms whereby these can happen.

21.5.2 Ion Exchange

It is possible to simply exchange one type of cationic species for another of equal charge without changing the ratio of cations to anions or introducing other defects in oxides. For example, the replacement of some or all of the sodium cations present in oxides by lithium cations is discussed in several places in this text.

Especially interesting is the exchange of lithium ions by protons. One method is chemically driven ion exchange, in which there is inter-diffusion in the solid state between native ionic species and ionic species from an adjacent liquid phase. An example of this is the replacement of lithium ions in an oxide solid electrolyte or mixed-conductor by protons as the result of immersion in an acidic aqueous solution. Protons from the solution diffuse into the oxide, replacing lithium ions, which move back into the solution. The presence of anions in the solution that react with lithium ions to form stable products, such as LiCl, can provide a strong driving force. An example could be a lithium transition metal oxide, $LiMO_2$ placed in an aqueous solution of HCl. In this case the ion exchange process can be written as a simple chemical reaction

$$HCl + LiMO_2 = HMO_2 + LiCl \tag{21.14}$$

The LiCl product can either remain in solution or precipitate as a solid product.

One can also use electrochemical methods to induce ion exchange. That is, one species inside a solid electrode can be replaced in the crystalline lattice by a different species from the electrolyte electrochemically. The species that is displaced leaves the solid and moves into the electrolyte or into another phase. This electrochemically-driven displacement process is now sometimes called "extrusion" by some investigators.

21.5.3 Simple Addition Methods

Instead of exchanging with lithium, hydrogen can be simply added to a solid in the form of interstitial protons. The charge balance requirement can be accomplished by the co-addition of either electronic or ionic species, i.e., either by the introduction of extra electrons or the introduction of negatively charged ionic species, such as O^{2-} ions. If electrons are introduced, the electrical potential of the material will become more negative, with a tendency toward n-type conductivity.

Similarly, oxygen, as oxide ions, can be introduced into solids, either directly from an adjacent gas phase or by reaction with water, with the concurrent formation of gaseous hydrogen molecules. Oxide ions can generally not reside upon interstitial sites in dense oxides because of their size, and thus their introduction requires the presence of oxygen vacancies in the crystal lattice. If only negatively charged oxide ions are introduced, electroneutrality requires the simultaneous introduction of electron holes. Thus the electrical potential of the solid becomes more positive, with a tendency toward p-type conductivity.

There is another possibility, first discussed by Stotz and Wagner [65, 66]. This is the simultaneous introduction of species related to both the hydrogen component and the oxygen component of water, i.e., both protons and oxide ions. This requires, of course, mechanisms for the transport of both hydrogen and oxygen species within the crystal structure. As mentioned already, hydrogen can enter the crystal structure of many oxides as mobile interstitial protons. The transport of oxide ions, that move by vacancy motion, requires the preexistence of oxide ion vacancies. This typically involves cation doping. In this dual mechanism the electrical charge is balanced. Neither electrons nor holes are involved, so the electrical potential of the solid is not changed. The concurrent introduction of both protons and oxide ions is, of course, compositionally equivalent to the addition of water to the solid, although the species H_2O does not actually exist in the crystal structure.

21.5.4 Thermodynamics of the Lithium: Hydrogen: Oxygen System

A number of the features of the interaction between lithium, hydrogen and oxygen in solids can be understood in terms of the thermodynamics of the ternary Li-H-O

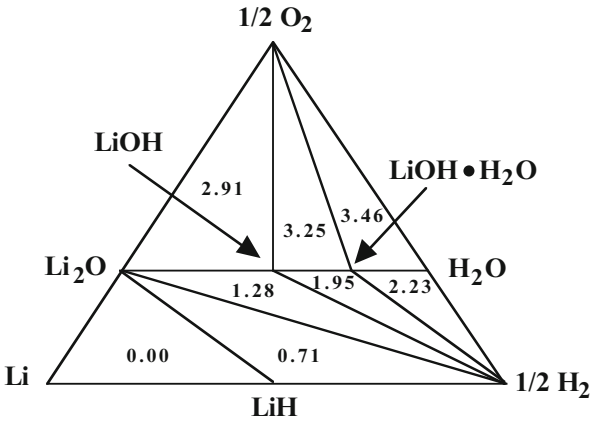

Fig. 21.24 Calculated phase stability diagram for the Li-H-O system at 298 K, assuming unit activities of all phases. The numbers within the triangles are their respective potentials vs. pure lithium. After ref. [66]

system. A useful thinking tool that can be used for this purpose is the *ternary phase stability diagram* with these three elements at the corners. This is discussed in some detail in Chap. 12.

The ternary phase stability diagram for the Li-H-O system at ambient temperature was determined [67] by using chemical thermodynamic data from Barin [68], and assuming that all relevant phases are in their standard states. An updated version is shown in Fig. 21.24.

Using the methods discussed in Chap. 11, the calculated voltages for the potentials of all compositions in the sub-triangles are shown relative to pure lithium.

If one considers an electrochemical cell with pure lithium at the negative electrode, the potential of water that is saturated with $LiOH \cdot H_2O$ will be 2.23 V when hydrogen is present at one atmosphere. On the other hand, water saturated with $LiOH \cdot H_2O$ will have a potential of 3.46 V vs. Li if one atmosphere of oxygen is present. It can be seen that under these conditions water has a stability window of 1.23 V, as is the case in the binary hydrogen–oxygen system.

These results may seem to be in conflict with the general conclusion in the literature that the potential of lithium is −3.05 V relative to that of the standard hydrogen electrode (SHE) potential in aqueous electrochemical systems. This can be reconciled by recognizing that the values calculated here are for the case that the water is in equilibrium with $LiOH \cdot H_2O$, which is very basic, with a pH of 14. The potentials of both the RHE and pure oxygen, as well as all other zero-degree-of-freedom equilibria, decrease by 0.059 V per pH unit. Thus, in order to be compared to the potential of the SHE, these calculated values have to be corrected by (14×0.59), or 0.826 V. Then the voltage between lithium and the SHE that is calculated in this way becomes 3.056 V, corresponding to the data in electrochemical tables.

21.5.5 Examples of Phases Containing Lithium That Are Stable in Water

A number of examples can be found in the literature that are consistent with, and illustrate these considerations. Particularly appropriate are several experimental results that were published by the group of J.R. Dahn some years ago.

They performed experiments on the addition of lithium to $LiMn_2O_4$ in a LiOH-containing aqueous electrolyte using a carbon negative electrode [69] and showed that the two-phase system $LiMn_2O_4$–$Li_2Mn_2O_4$, that is known to have a potential of 2.97 V vs. Li in nonaqueous cells [70] is stable in water containing LiOH. They used a Ag/AgCl reference electrode, referred their measurements to the SHE, and then converted to the lithium scale, assuming that the potential of the lithium electrode is −3.05 V vs. the SHE. They found that lithium began reacting with the $LiMn_2O_4$ at a potential of −0.1 V vs. the SHE, which is consistent with the value of 2.97 V vs. Li mentioned above.

As lithium was added beyond the two-phase composition limit the potential fell to that for hydrogen evolution. Their data showed hydrogen evolution at a potential 2.2 V vs. pure Li, and found oxygen evolution on a carbon negative electrode at 3.4 V vs. pure Li. It can readily be seen that these experimental results are consistent with the results of the Gibbs triangle calculations shown in Fig. 21.23.

It was also found that the phase VO_2(B) reacts with lithium at potentials within the stability range of water [71]. Electrochemical cell experiments were performed in which Li_xVO_2(B) acted as the negative electrode, and $Li_xMn_2O_4$ as the positive electrode [72]. These aqueous electrolyte cells gave comparable results to those with the same electrodes in organic solvent electrolyte cells.

21.5.6 Materials That Have Potentials Above the Stability Window of Water

At normal pressures materials with potentials more positive than that of pure oxygen will tend to oxidize water to cause the evolution of electrically neutral molecular oxygen gas. For this to happen there must be a concurrent reduction process. One possibility is the insertion of positively charged ionic species, along with their charge-balancing electrons, into the material in question. The insertion of protons or lithium ions and electrons into high-potential oxides is one possible example of such a reduction process. When this happens, the potential of the material goes down toward that of pure oxygen.

21.5.7 Absorption of Protons from Water Vapor in the Atmosphere

A number of materials that are used as positive electrode reactants in lithium battery systems have operating potentials well above the stability range of water. Cells containing these materials and carbon negative electrodes are typically assembled in air in the uncharged state. It is generally found that the open circuit cell voltage at the start of the first charge is consistent with lithium–air equilibrium, i.e., along the Li_2O/O_2 edge of the ternary phase stability diagram in Fig. 21.1. This can be calculated to be 2.91 V vs. pure lithium. This can be explained by the reaction of these materials with water vapor in the atmosphere. Protons and electrons enter the crystal structures of these high potential materials, reducing their potentials to that value. This is accompanied by the concurrent evolution of molecular oxygen.

21.5.8 Extraction of Lithium from Aqueous Solutions

An analogous situation can occur if a material that can readily insert lithium, rather than protons, has a potential above the stability range of water. If lithium ions and electrons enter the material's structure the potential will decrease until the value in equilibrium with oxygen is reached. Such a material can thus be used to extract lithium from aqueous solutions. This was demonstrated by experiments on the use of the λ-MnO_2 spinel phase that absorbed lithium when it was immersed in aqueous chloride solutions [73].

References

1. Yao YFY, Kummer JT (1967) J Inorg Nucl Chem 29:2453
2. Weber N, Kummer JT. (1967) Proceedings Annual Power Sources Conference 21, 37
3. Coetzer J (1986) J Power Sources 18:377
4. Galloway RC (1987) J Electrochem Soc 134:256
5. Bones RJ, Coetzer J, Galloway RC, Teagle DA (1987) J Electrochem Soc 134:2379
6. Huggins RA (1999) J Power Sources 81–82:13
7. Vissers DR, Tomczuk Z, Steunenberg RK (1974) J Electrochem Soc 121:665
8. Whittingham MS (1976) Science 192:1126
9. Whittingham MS (1976) J Electrochem Soc 123:315
10. Whittingham MS (1993) Intercalation Compounds. In: Scrosati B, Magistris A, Mari CM, Mariotto G (eds) Fast Ion Transport. KluwerAcademic Publishers, Dordrecht, p 69
11. Dickens PG, French SJ, Hight AT, Pye MF (1979) Mater Res Bull 14:1295
12. Mizushima K, Jones PC, Wiseman PJ, Goodenough JB (1980) Mater Res Bull 15:783
13. Goodenough JB, Mizushima K, Takada T (1980) Jpn J Appl Phys 19(Supplement 19-3):305
14. Nagaura T, Tozawa K (1990) Progress in Batteries and Solar Cells, vol 9. JEC Press, Inc, Brunswick, OH, p 209

15. Nagaura T (1991) Progress in Batteries and Solar Cells, vol 10. JEC Press, Inc, Brunswick, OH, p 218
16. Yamada A, Hosoya M, Chung SC, Kudo Y, Liu KY. (2001) Abstract No. 205, Electrochemical Society Meeting, San Francisco
17. Nanjundaswamy KS, Padhi AK, Goodenough JB, Okada S, Ohtsuka H, Arai H, Yamaki J (1996) Solid State Ionics 92:1
18. Padhi AK, Nanjundaswamy KS, Masquelier C, Goodenough JB (1997) J Electrochem Soc 144:2581
19. Okada S, Ohtsuka H, Arai H, Ichimura M (1993) Electrochem. Soc Ext Abstracts 93–1:130
20. Okada S, Takada T, Egashira M, Yamaki J, Tabuchi M, Kageyama H, Kodama T, Kanno R. (1999) Presented at Second Hawaii Battery Conference, Jan. 1999
21. Sadadone I, Delmas C (1996) J Mater Chem 6:193
22. Bruce PG, Armstrong AR, Gitzendanner R (1999) J Mater Chem 9:193
23. Grincourt Y, Storey C, Davidson IJ (2001) J Power Sources 97–98:711
24. Paulson JM, Donaberger RA, Dahn JR (2000) Chem Mater 12:2257
25. Spahr ME, Novak P, Schneider B, Haas O, Nesper RJ (1998) J Electrochem Soc 145:1113
26. Ohzuku T, Makimura Y (2001) Chem Lett 8:744
27. Lu Z, MacNeil DD, Dahn JR (2001) Electrochem Solid-State Lett 4:A191
28. Kang K, Meng YS, Breger J, Grey CP, Ceder G (2006) Science 311:977
29. Liu Z, Yu A, Lee JY (1999) J Power Sources 81–82:416
30. Yoshio M, Noguchi H, Itoh J-I, Okada M, Mouri T (2000) J Power Sources 90:176
31. Whittingham MS (2004) Chem Rev 104:4271
32. Thackeray MM, David WIF, Bruce PG, Goodenough JB (1983) Mater Res Bull 18:461
33. Thackeray MM, Johnson PJ, de Piciotto LA, Bruce PG, Goodenough JB (1984) Mater Res Bull 19:179
34. Thackeray MM. (1999) In: Handbook of Battery Materials. JO. Besenhard (ed.), Wiley-VCH p. 293
35. Guyomard D, Tarascon JM (1994) Solid State Ionics 69:222
36. Amatucci G, Tarascon J-M (2002) J Electrochem Soc 149:K31
37. Gummow RJ, De Kock A, Thackeray MM (1994) Solid State Ionics 69:59
38. Guyomard D, Tarascon J-M. US Patent 5,192,629, (March 9, 1993)
39. Guyomard D, Tarascon J-M (1994) Solid State Ionics 69:293
40. Sigala C, Guyomard D, Verbaere A, Piffard Y, Tournoux M (1995) Solid State Ionics 81:167
41. Ein-Eli Y, Howard WF (1997) J Electrochem Soc 144:L205
42. Ein-Eli Y, Howard WF, Lu SH, Mukerjee S, McBreen J, Vaughey JT, Thackeray MM (1998) J Electrochem Soc 145:1238
43. Ein-Eli Y, Lu SH, Rzeznik MA, Mukerjee S, Yang XQ, McBreen J (1998) J Electrochem Soc 145:3383
44. Ohzuku T, Takeda S, Iwanaga M (1999) J Power Sources 81–82:90
45. Ariyoshi K, Iwakoshi Y, Nakayama N, Ohzuku T (2004) J Electrochem Soc 151:A296
46. Colbow KM, Dahn JR, Haering RR (1989) J Power Sources 26:397
47. Ohzuku T, Ueda A, Yamamoto N (1995) J Electrochem Soc 142:1431
48. Goodenough JB, Hong HY-P, Kafalas JA (1976) Mater Res Bull 11:203
49. Padhi AK, Nanjundaswamy KS, Masquelier C, Okada S, Goodenough JB (1997) J Electrochem Soc 144:1609
50. Barker J, Saidi MY. US Patent 5,871,866 (1999)
51. Saıdi MY, Barker J, Huang H, Swoyer JL, Adamson G (2002) Electrochem Solid-State Lett 5: A149
52. Padhi AK, Nanjundaswamy KS, Goodenough JB (1997) J Electrochem Soc 144:1188
53. Ravet N, Goodenough JB, Besner S, Simoneau M. Hovington P, Armand M (1999) Electrochem. Soc. Meeting Abstract 99-2, 127
54. Chung S-Y, Bloking JT, Chiang Y-M (2002) Nat Mater 1:123
55. Amin R, Maier J (2008) Solid State Ionics 178:1831

56. Herle PS, Ellis B, Coombs N, Nazar LF (2004) Nat Mater 3:147
57. Ong SP, Wang L, Kang B, Ceder G. Presented at the Materials Research Society Meeting in San Francisco, March, 2007
58. Meethong N, Huang H-YS, Speakman SA, Carter WC, Chiang Y-M (2007) Adv Funct Mater 17:1115
59. Barker J, Saidi MY, Swoyer JL (2004) J Electrochem Soc 151:A1670
60. Barker J, Gover RKB, Burns P, Bryan AJ (2007) Electrochem Solid-State Lett 10:A130
61. Barker J, Gover RKB, Burns P, Bryan AJ (2006) Electrochem Solid-State Lett 9:A190
62. Barker J, Gover RKB, Burns P, Bryan AJ (2007) J Electrochem Soc 154:A882
63. Dahn JR, Fuller EW, Obrovac M, von Sacken U (1994) Solid State Ionics 69:265
64. Godshall NA, Raistrick ID, Huggins RA (1984) J Electrochem Soc 131:543
65. Stotz S, Wagner C (1966) Ber Bunsenges Physik Chem 70:781
66. Wagner C (1968) Ber Bunsenges Physik Chem 72:778
67. Huggins RA (2000) Solid State Ionics 136–137:1321
68. Barin I. Thermochemical Data of Pure Substances. 3rd Edition, VCH 1995, Published Online 24 Apr 2008, ISBN 9783527619825
69. Dahn JR, von Sacken U, Al-Janaby H, Juzkow MW (1991) J Electrochem Soc 138:2207
70. Li W, McKinnon WR, Dahn JR (1994) J Electrochem Soc 141:2310
71. Tarascon JM, Guyomard D (1993) J Electrochem Soc 138:2864
72. Li W, Dahn JR (1995) J Electrochem Soc 142:1742
73. Kanoh H, Ooi K, Miyai Y, Katoh S (1993) Sep Sci Technol 28:643